nature communications

Article

https://doi.org/10.1038/s41467-024-50532-5

Thermal disorder prevents the suppression of ultra-fast photochemistry in the strong light-matter coupling regime

Received: 22 August 2023

Accepted: 11 July 2024

Arpan Dutta[1,4], Ville Tiainen[1], Ilia Sokolovskii[2], Luís Duarte[1,5], Nemanja Markešević[1,6], Dmitry Morozov[2], Hassan A. Qureshi[1,4], Siim Pikker[1,3], Gerrit Groenhof[2] & J. Jussi Toppari[1]

Strong coupling between molecules and confined light modes of optical cavities to form polaritons can alter photochemistry, but the origin of this effect remains largely unknown. While theoretical models suggest a suppression of photochemistry due to the formation of new polaritonic potential energy surfaces, many of these models do not account for the energetic disorder among the molecules, which is unavoidable at ambient conditions. Here, we combine simulations and experiments to show that for an ultra-fast photochemical reaction such thermal disorder prevents the modification of the potential energy surface and that suppression is due to radiative decay of the lossy cavity modes. We also show that the excitation spectrum under strong coupling is a product of the excitation spectrum of the bare molecules and the absorption spectrum of the molecule-cavity system, suggesting that polaritons can act as gateways for channeling an excitation into a molecule, which then reacts normally. Our results therefore imply that strong coupling provides a means to tune the action spectrum of a molecule, rather than to change the reaction.

Placing molecules between the mirrors of a Fabry–Pérot micro-cavity that is resonant with their excitation frequency, has been shown to alter their chemistry in both ground and excited states[1–9], but the origin of these effects is hitherto unknown. Inside the cavity, the rate of energy exchange between excitations of the molecules and confined light modes of the cavity can exceed the intrinsic decay rates of both the molecular excitations and the photonic modes[10]. Under these conditions, the system enters the strong light-matter coupling regime, in which the excitations of the molecules hybridize with the confined light modes of the cavity to form new light-matter states, called polaritons[11–14].

Changes to photo-chemical reactivity have been rationalized on the basis of differences between the potential energy surfaces of the polariton and that of the bare molecule, as illustrated in Fig. 1c[15]. The key to this hypothesis is that the lifetime of the polariton is sufficiently long for the reactants to evolve over the modified portions of the potential energy surface. Despite recent suggestions that the lowest-energy polariton state can be very long-lived[16], polariton lifetimes are generally considered to be limited by the lifetime of the cavity photon[17,18], which is on the order of a few tens of femtoseconds in the metallic cavities that have been used in experiments. Because the polariton decay rate in these experiments was significantly higher than

---

[1]Nanoscience Center and Department of Physics, University of Jyväskylä, P.O. Box 35, 40014 Jyväskylä, Finland. [2]Nanoscience Center and Department of Chemistry, University of Jyväskylä, P.O. Box 35, 40014 Jyväskylä, Finland. [3]Institute of Physics, University of Tartu, W. Ostwaldi 1, 50411 Tartu, Estonia. [4]Present address: Department of Mechanical and Materials Engineering, University of Turku, 20014 Turku, Finland. [5]Present address: Department of Chemistry, University of Helsinki, P.O. Box 55, 00014 Helsinki, Finland. [6]Present address: CNR-INO Istituto Nazionale di Ottica del Consiglio Nazionale delle Ricerche and LENS European Laboratory for Nonlinear Spectroscopy, Via Nello Carrara 1, Sesto Fiorentino 50019, Italy. e-mail: gerrit.x.groenhof@jyu.fi; j.jussi.toppari@jyu.fi

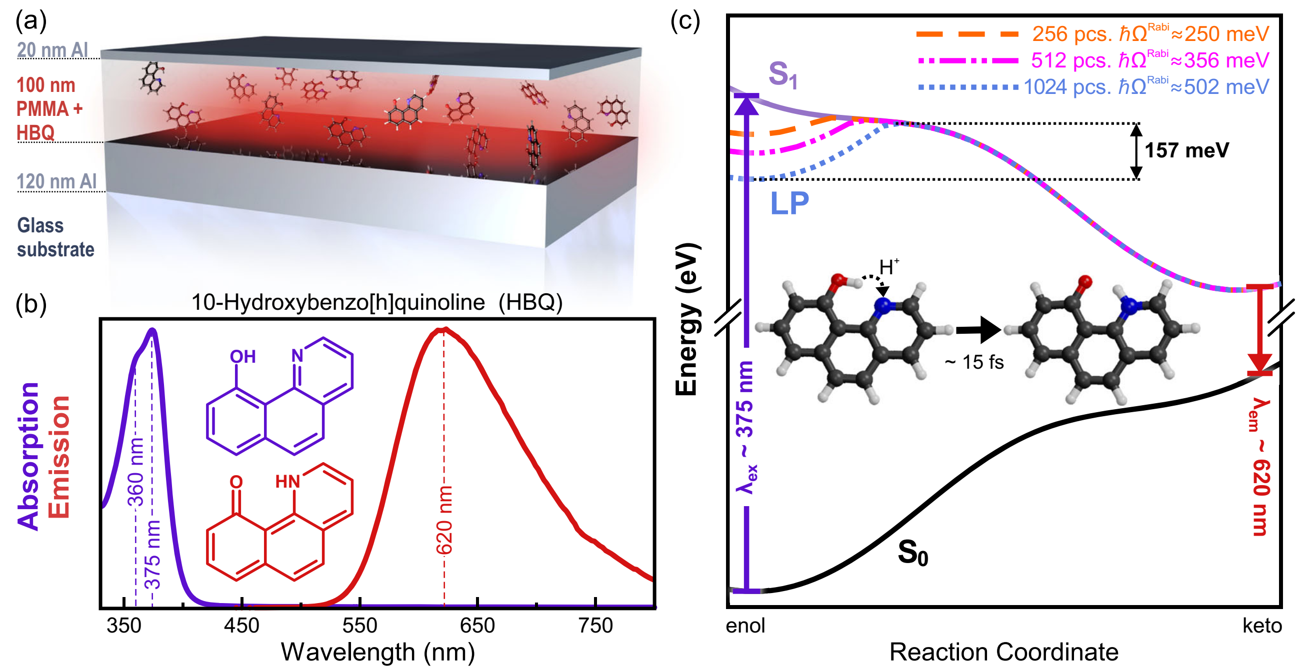

Fig. 1 | Proposed mechanism for suppression of ultra-fast photochemistry due to collective strong coupling in optical cavities. a Schematic illustration of the cavity geometry (not to scale). **b** Normalized absorption and emission spectra of HBQ in PMMA films. **c** Potential energy profiles for intra-molecular proton transfer in the electronic ground state (S_0, black), first singlet electronic excited state (S_1, purple), and in the lower polariton (LP), when 256 (orange dashed), 512 (magenta dashed-dotted) or 1024 (blue dotted) identical HBQ molecules are strongly coupled to a single confined light mode of an optical cavity that is resonant with the $S_0 \rightarrow S_1$ transition in HBQ shown as a purple upwards arrow. The Rabi splittings, $\hbar\Omega^{\mathrm{Rabi}}$, are listed in the upper right corner. The 157 meV energy barrier for proton transfer in the LP state with highest Rabi split is indicated by the black double-arrow. The emission of the photoproduct after the proton transfer is shown as a red downwards arrow. Source data are provided as a Source Data file.

the rate of the photo-chemical reaction[1,6,7,9], it remains difficult to understand whether the observed changes in reactivity are due to the polaritonic states providing (1) a competing radiative decay channel[8], (2) a different potential energy surface[15], or (3) a combination of both.

To disentangle these effects, and understand how strong coupling affects photo-reactivity, experiments should instead be performed on a photo-chemical reaction that happens at same timescale as polariton decay. In this work, we therefore investigated the influence of strong light-matter coupling on the ultra-fast photochemical reaction of 10-hydroxybenzo[h]quinoline (HBQ) in an optical cavity (Fig. 1a). The reaction in the electronic excited-state (S_1) of this molecule happens on a timescale of ~15 fs[19,20], which is comparable to the lifetime of a cavity photon in metallic micro-cavities.

Figure 1b shows the normalized absorption and emission spectra of HBQ in polymethyl methacrylate (PMMA), which we used as a polymer matrix for embedding the molecules within the cavity (Fig. 1a). Photon absorption at 375 nm triggers an ultra-fast excited state intra-molecular proton transfer (ESIPT) from the phenol oxygen to the nitrogen atom[19,20], as shown in Fig. 1c. The reaction coordinate is defined as the difference between the Oxygen-Hydrogen and Nitrogen-Hydrogen distances: $d_{\text{O-H}} - d_{\text{N-H}}$. After proton transfer, the keto-form of HBQ decays back to the electronic ground state (S_0) through photon emission with a maximum around 620 nm.

Results from density functional theory (DFT) calculations at the TDA-CAM-B3LYP/6-31G* level of theory[21–24] suggest that outside of the cavity, proton transfer is a barrier-less process in the first singlet electronic excited state (S_1, Fig. 1c). When N molecules are placed inside the cavity, the $S_0 \rightarrow S_1$ excitations couple to the confined light modes that are resonant with the excitation energy (375 nm in experiment, 305 nm at the TDA-CAM-B3LYP/6-31G* level of theory, see below), to form the upper (UP) and lower (LP) polaritons, as well as $N-1$ dark states. The Rabi splitting that separates the LP and UP states, creates a local minimum on the potential energy surface of the LP state[15]. As a consequence, the excited-state intra-molecular proton transfer in the lowest-energy excited state of the molecule-cavity system is no longer barrier-less (Fig. 1c). Because the Rabi splitting depends on the molecular concentration, i.e., $\hbar\Omega^{\mathrm{Rabi}} \propto \sqrt{N/V_{\mathrm{cav}}}$[14], we can control the barrier separating the local minimum on the LP surface from the product minimum by varying the number of molecules in the cavity mode volume (V_{cav}), as illustrated in Fig. 1c, and thus systematically reduce the proton transfer rate. This reduction, in combination with the low LP lifetime, should hence suppress the emission at 620 nm, which is sufficiently far off-resonance from the lowest-frequency cavity mode to be affected by strong coupling or Purcell enhancement.

Because the potential energy profiles, shown in Fig. 1c, for excited-state intra-molecular proton transfer in one of the HBQ molecules, were computed while keeping the other $N-1$ molecules in their S_0 minimum energy geometries, thermal disorder was neglected. To test if the suppression hypothesis[15] is valid also when there is disorder, we performed both molecular dynamics (MD) simulations and experiments at room temperature.

Here, we show that thermal disorder at room temperature prevents the suppression of the ultra-fast proton transfer reaction in the strong coupling regime. Because the thermal disorder redistributes the cavity mode contribution over all eigenstates, the distinction between polaritonic and dark states vanishes, and all states become gray. As these gray states are dominated by electronic excitations localized on the molecules, the modifications of the potential energy surfaces due to the strong light-matter coupling, are too small to prevent proton transfer.

Results and discussion

In the simulations, the details of which can be found in the “Methods” section and in the Supplementary Information (section 2), 512 HBQ molecules solvated in cyclohexane, were placed inside a single-mode

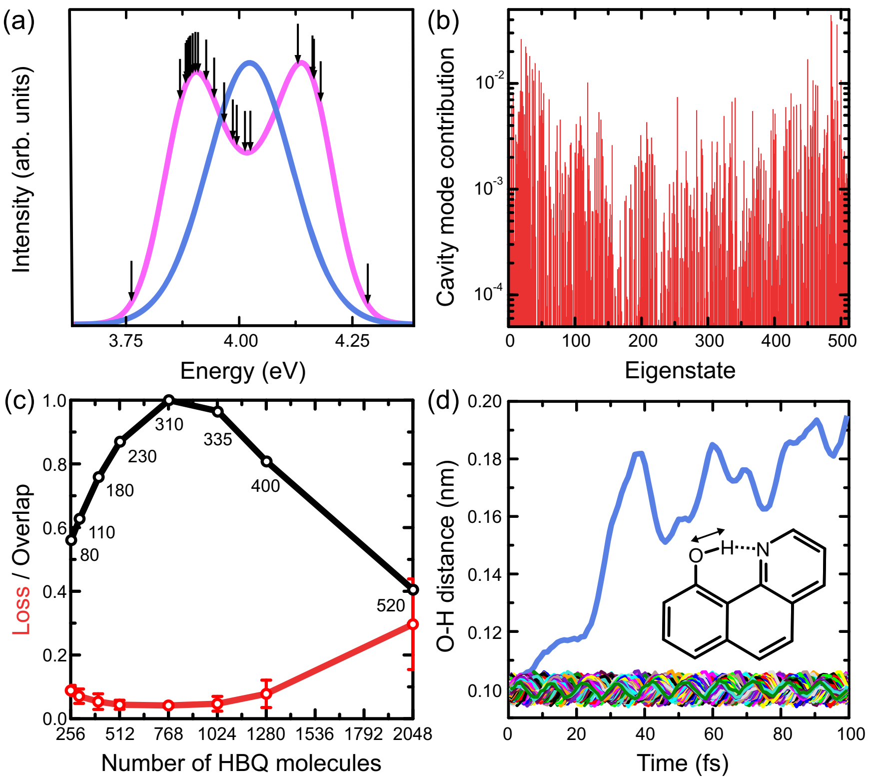

Fig. 2 | Results of molecular dynamics simulations of HBQ molecules collectively coupled to a cavity. **a** Absorption spectra of HBQ in cyclohexane at 300 K outside (blue) and of 512 HBQ molecules inside (magenta) a single-mode microcavity that is resonant with the absorption maximum of HBQ (4.02 eV at the CAM-B3LYP/6-31G(d)//Gromos96 level of hybrid quantum mechanics/molecular mechanics (QM/MM) theory). Arrows indicate the eigenstates in which molecular dynamics simulations were started. **b** Contribution of the cavity mode ($|\alpha^m|^2$, Eq. (S16), Supplementary Information) to the eigenstates of the coupled HBQ-cavity system. **c** Overlap between the polaritonic absorption spectrum and the molecular density of states as a function of the number of strongly-coupled molecules (black). The red line shows the losses due to cavity decay. Data are presented as mean values ± standard deviation, obtained from all trajectories performed for a specific number of molecules (see Supplementary Information 2.7.2 for an overview of the number of trajectories for each HBQ ensemble size). The numbers under the black data points give the Rabi splitting in meV. **d** Time evolution of the O-H distances in each of the 512 strongly-coupled HBQ molecules (all colors) after excitation into an optically bright polaritonic state (i.e., state 19, second arrow from left in (**a**)). As schematically illustrated in the inset, the OH distance is the reaction coordinate for excited-state intra-molecular proton transfer, and a distance of ~0.10 nm corresponds to the situation where the proton is bound to the phenol oxygen, whereas a distance around 0.19 nm indicates that the reaction has occurred and the proton has transferred to the nitrogen. Here, the latter happened in molecule 400, for which the OH distance is shown in blue. Source data are provided as a Source Data file.

cavity. The configurations of these molecules were extracted from a classical MD trajectory in the electronic ground state, which sampled the Boltzmann distribution at 300 K[25]. The energy of the cavity mode was resonant with the absorption maximum of our molecular model (see below) at $\hbar\omega_{\mathrm{cav}} = 4.02$ eV. In all simulations, the strength of the vacuum field was $\sqrt{\hbar\omega_{\mathrm{cav}}/2\epsilon_0 V_{\mathrm{cav}}} = 0.77\,\mathrm{MV\,cm^{-1}}$. With only 512 molecules coupled to the cavity mode, this field needs to be stronger than in experiments, where the collective coupling regime is typically achieved with 10^5 molecules or more[26–29].

As shown in Fig. 2a, the calculated QM/MM $S_0 \rightarrow S_1$ absorption spectrum of HBQ at 300 K (Supplementary Information, subsection 2.5) splits inside the cavity, suggesting that the molecule-cavity system is in the strong coupling regime with a Rabi splitting of 230 meV. We performed 22 MD simulations, starting in different adiabatic eigenstates of the molecule-cavity system, that are indicated by arrows in Fig. 2a. In all simulations, intra-molecular proton transfer occurs irrespective of the polaritonic eigenstate that was initially excited (Fig. S13b, Supplementary Information). In Fig. 2d, we plot the O-H distances of the 512 strongly coupled HBQ molecules in one of the trajectories. In this trajectory, a proton transfer reaction occurs in HBQ molecule 400 within 25 fs after excitation into the 19th eigenstate, as indicated by an increase of the O-H distance (blue curve). The other 511 molecules remain in their ground state geometries, sampling O-H bond distances around the S_0 equilibrium value of 0.1 nm. Because the reaction rate in QM/MM simulations of HBQ outside of the cavity is very similar (Fig. S13a, Supplementary Information), these results suggest that strong coupling does not have an appreciable effect on the reaction. Thus, even though the Rabi splitting implies strong coupling, the formation of polaritonic states does not lead to a suppression of the photo-chemical reaction in HBQ, in contrast to theoretical predictions[15], and experiments on spiropyran and norbornadiene in Fabry–Pérot cavities[1,9,30,31], nor to an acceleration, as observed in experiments on fulgide photo-switching in an optical cavity[32].

To understand why excitation into a polaritonic eigenstate of the molecule-cavity system does not suppress the reactivity in our simulations, we inspected the composition of these states. As shown in Fig. 2b, the cavity mode is distributed over virtually all eigenstates of the molecule-cavity system. As pointed out by Houdré et al.[26] for atoms, and later by Mony et al.[9] for molecules, this is due to structural, and hence energetic disorder among the HBQ molecules at 300 K. Without disorder, only the optically accessible upper and lower polariton states include contribution of the cavity mode and thus have a different potential energy surface on which reactivity can be suppressed (Fig. 1). The other $N-1$ eigenstates are dark, i.e., without contribution from the cavity mode, and have potential energy surfaces that are similar to the S_1 surface of the uncoupled molecule. In contrast, when there is disorder, which is unavoidable in experiments under ambient conditions, all states are optically accessible, but because molecular excitations dominate these states, rather than the cavity mode, the potential energy surfaces are hardly perturbed with respect to the bare molecules—not even for the brightest polaritonic states.

In our simulations, a perfect cavity was assumed, without any losses. However, in reality, photon leakage through the mirrors is unavoidable and hence provides an additional decay channel for the excited population that could reduce the quantum yield and hence suppress the reaction. Under the assumption that the rate of radiative decay during an MD timestep, Δt, from a polaritonic state is proportional to its cavity mode contribution[18,33,34], we accounted for such reduction in the quantum yield a posteriori by recomputing the evolution of the polaritonic wave function under the influence of cavity losses along the MD trajectories (Supplementary Information, subsection 2.4). In these calculations we assumed a cavity decay rate of $\gamma_{\text{cav}} = 250\,\text{ps}^{-1}$, which is typical for a low quality metallic cavity with $Q \sim 15$. The losses estimated under these assumptions, plotted for various ensemble sizes in Fig. 2c, suggest an average loss of only 5% for the 512 molecule-cavity system.

The extent of the radiative loss depends on how rapidly the population transfers from a bright polaritonic state with cavity mode contribution and hence susceptible to radiative decay, into a dark state that is localized on a single molecule and therefore lacks cavity mode contribution[35,36]. Because the rate of this non-adiabatic population transfer process is inversely proportional to the energy difference between the states[37], the radiative loss depends on the overlap between the optically-bright states and the molecular dark states[18]. Because that overlap is determined by the Rabi splitting, the loss can be controlled by varying the HBQ concentration[18].

However, because adding more molecules inside the cavity mode volume not only increases the Rabi splitting, but also the number of dark states, the overlap between the polaritonic absorption spectrum (Fig. 2a), which represents the distribution of the optically-bright states (Fig. 2b), on the one hand, and the molecular absorption spectrum, which represents the distribution of the molecular dark states[18], on the other hand, has a maximum at a specific Rabi splitting, or equivalently, a specific number of molecules, as shown in Fig. 2c. Therefore, also the suppression of the reaction due to radiative loss has a minimum around that Rabi splitting and increases again at higher concentrations. Losses estimated for simulations with a different number of molecules in the same cavity, confirm this correlation between Rabi splitting and losses, at least qualitatively (Fig. 2c).

With 2048 HBQ molecules in the cavity and a collective Rabi splitting of 520 meV, the losses reduce the formation of the photoproduct by 30%, in line with a smaller overlap. To remove the overlap and hence suppress photo-product emission, the Rabi splitting must exceed 800 meV (Supplementary Information, Fig. S15), placing the system in the ultra-strong coupling regime. Such coupling strengths are not only challenging to achieve experimentally due to the limited solubility of HBQ in PMMA, but also difficult to simulate, as the rotating wave approximation (RWA), on which our model is based[33], may loose its validity in this regime[38]. Notwithstanding the potential limitations of the RWA, we observed full suppression of the reaction in simulations at a Rabi splitting of 820 meV (Fig. S15b).

Summarizing, the results of our calculations suggest that within the strong coupling regime, the thermal disorder at 300 K prevents the modification of the potential energy surfaces, in line with recent results from quantum dynamics simulations[39] and experiments[30,31,40]. Instead, ultra-strong coupling would be required to create a polaritonic potential energy surface with a sufficiently deep local minimum to reduce the reaction rate. In both regimes, cavity decay provides a competing loss channel that suppresses the overall reaction quantum yield and our calculations suggest that the extent of such suppression can be tuned via the HBQ concentration (Fig. 2c).

To verify the validity of these findings experimentally, we fabricated metallic Fabry–Pérot micro-cavities containing HBQ molecules and measured the photo-luminescence associated with the photo-product at 620 nm as a function of light-matter coupling strength and excitation wavelength. As shown schematically in Fig. 1a, a ~100 nm PMMA film doped with HBQ, was covered with a 20 nm thick semitransparent aluminum (Al) mirror on top and a 120 nm non-transparent Al mirror on the bottom[41]. The top mirror is sufficiently thin for the HBQ photo-product emission around 620 nm to leak through and be detected. The thickness of the cavities was tuned to match the first-order cavity mode with the HBQ absorption maximum at 375 nm. To control the collective light-matter coupling strength ($\propto \sqrt{N}$), we varied the concentration of HBQ in the PMMA film. Because the first-order cavity mode is sufficiently higher in energy than the emission maximum of the HBQ photo-product, we can exclude fluorescence enhancement due to the Purcell effect[42]. Further details on the design, fabrication and characterization of the cavity systems are provided in the Supplementary Information (section 1).

Three micro-cavities were fabricated with HBQ/PMMA ratios of 0.5 (low), 1.0 (mid), and 1.6 (high concentration). In addition, three bare films were fabricated with the same HBQ/PMMA ratios as in the cavities. To provide a similar geometry for the reflection measurements, these films were also deposited on a 120 nm thick non-transparent Al mirror, i.e., the structure was identical to the cavity geometry shown in Fig. 1a except for the top mirror.

We measured angle-dependent steady-state absorption spectra of the cavities, which are shown as contour maps in Fig. 3. The anticrossings between the bright polaritonic branches around 40°–50° incident angle, suggest that the cavities are in the strong coupling regime and that the first-order cavity mode is hybridized with the two lowest-energy electronic transitions in HBQ, namely the main peak at 375 nm and the (vibronic) shoulder at 360 nm (Fig. 1b). These molecular transitions are shown as black dotted horizontal lines, together with the complete absorption spectrum of the HBQ/PMMA film in pink. The energies of LP and UP, extracted from the angle-resolved experimental spectra, are shown as black crosses.

While in previous works on strong coupling with organic molecules, coupling strengths and cavity mode dispersions were often extracted from the measured spectra by means of the coupled harmonic oscillator model (CHOM)[9,13,32,43–45], a straightforward application of this model to our reflectivity data is compromised by the limited visibility of the Middle Polariton (MP), situated between the two vibronic transitions of HBQ. The limited visibility of this MP is due the heterogeneous broadening of the transitions[46]. As demonstrated by Musser et al., applying the CHOM to organic molecules with broad absorption spectra, provides coupling constants, g, that do not reflect the actual strength of the light-matter interaction[46]. Therefore, criteria for strong coupling based on the coupling constants obtained from a fit of the CHOM to the experimental data (i.e., $2g \geq \kappa_{\text{mol}} + \gamma_{\text{cav}}$, with κ_{mol} and γ_{cav} the decay rates of the molecule and the cavity, respectively), cannot be used to determine if our system is in the strong coupling regime.

We, therefore, instead focus on the observable splitting of the molecular absorption into clearly visible upper and lower branches with dispersion, and report the minimum energy gap between these branches in Table 1 as a proxy for the coupling strength. Because this gap, which is similar to the Rabi splitting of 240 meV in the MD simulations, scales with the expected square-root of the molecular concentration in all samples[46], we consider our systems to be in the strong coupling regime. Although the CHOM may not be very suitable for extracting the coupling strengths, we nevertheless used it to visualize the polariton dispersions and to estimate the cavity dispersion, shown as white dashed lines and black dotted lines, respectively, in the spectra of Fig. 3.

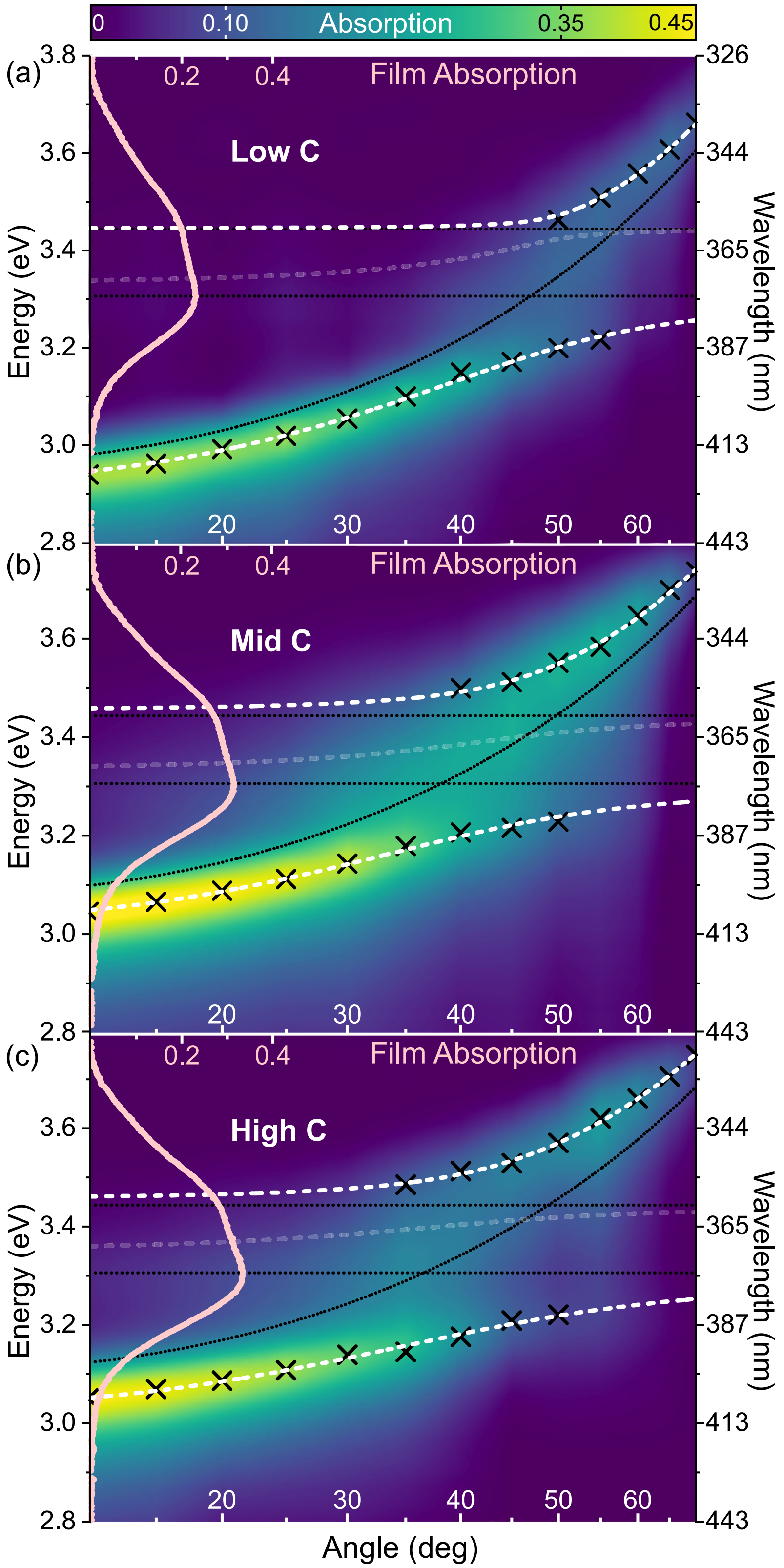

Fig. 3 | Measured and modeled dispersions of strongly coupled HBQ cavities. Angle-resolved absorption (contour map) of cavities containing HBQ at (**a**) low, (**b**) mid, and (**c**) high concentration (C). The absorption spectra of the bare HBQ/PMMA films are shown in pink on the left axis. The white dashed curves represent the upper, middle, and lower polariton branches obtained from fitting the coupled harmonic oscillator model (CHOM, Supplementary Information, subsection 1.7) to the measured spectral positions (black crosses). The middle polariton branches were too faint to be resolved, and therefore not included in the fitting. The black dotted curves depict the dispersion of an undoped cavity (i.e., containing only PMMA), while the horizontal black dotted lines show the molecular absorption peaks at 360 nm and 375 nm of HBQ. Source data are provided as a Source Data file.

Table 1 | Energy difference between the upper (UP) and lower polariton (LP) for cavities with low, mid and high concentration (C)

C	HBQ/PMMA	UP-LP (meV)	θ_{res} (deg)	λ_{res} (nm)
Low	0.5	~270	50	385
Mid	1	~290	40	386
High	1.6	~325	40	390

The concentrations are defined as the HBQ/PMMA weight ratios (second column), at the incidence angle for which the cavity dispersion and HBQ absorption are maximum are resonant (θ_{res}, fourth column). The last column lists the wavelength of the LP absorption maximum (λ_{res}) at these angles.

To verify the main finding in our simulations that exciting any eigenstate of the molecule-cavity system leads to proton transfer and the formation of the photo-product, we recorded cavity excitation spectra by measuring the intensity of the steady-state emission of the photo-product at 620 nm as a function of excitation wavelength and angle. Since the energy gap between the lower polariton and the fluorescence spectrum of HBQ (Fig. 1b) is more than an eV at all angles, we can rule out photo-product emission through the optically transparent polaritonic branches. The cavity system was excited with ~5 ns pulses at a 100 Hz repetition rate from a tunable laser source. Because the fluorescence is emitted from uncoupled molecules without angular dependence, the emission was always collected at the sample surface normal (i.e., at 0°).

The observation that the yield of the reaction in our simulations depends on the overlap between bright and dark states (Fig. 2c)[18], suggests that the excitation spectra of the HBQ-cavity systems can be obtained by multiplying the probability to absorb a photon, determined by the absorption spectrum of the HBQ cavity, and the probability to undergo ESIPT, which is determined by the density of molecular states. Because for HBQ the absorption and excitation spectra are the same in solution (Supplementary Information, Fig. S3) and very similar in the PMMA film (Supplementary Information, Fig. S4), we obtained this density of states by measuring the excitation spectra of the HBQ/PMMA films.

In Fig. 4, we show the absorption spectra (a,b) and excitation spectra (c,d) at various incidence angles for the mid C (left column) and the high C (right column) HBQ/PMMA cavities, as well as the excitation spectra of films with the same HBQ/PMMA doping ratios as the cavities (c,d). The qualitative agreement between the measured cavity excitation spectra (Fig. 4c, d), on the one hand, and the spectra obtained by multiplying the cavity absorption spectra and film excitation spectra (Fig. 4e, f), on the other hand, confirm the results from the simulations that the efficiency of the reaction is primarily controlled by the overlap between the bright polaritons and the molecular dark states. Likewise, dividing the excitation spectra of the HBQ/PMMA-cavity systems by the excitation spectra of the HBQ/PMMA films, yields the polaritonic absorption spectra (Fig. 4g, h), affirming our conjecture. We note that the agreement between the calculated and measured spectra is not perfect for all angles, which we attribute to uncertainties in the baseline corrections that were applied to the cavity absorption spectra (Supplementary Information, Section 1.4).

Additional support is provided by the lower yield of the photo-product emission at the largest angles where the overlap between the polaritonic absorption maxima and film excitation spectrum is smallest. Simulations, in which the cavity is red-detuned to mimic excitation at such angles, confirm this (Supplementary Information, Fig. S14). Thus, the results of both our MD simulations and excitation spectra measurements suggest that in the strong coupling regime the bright polaritonic states act as a gate-way to access the reactive dark states and that the efficiency of this gate-way, or optical filter, depends on the overlap between the polaritonic absorption spectrum and the molecular density of states[18].

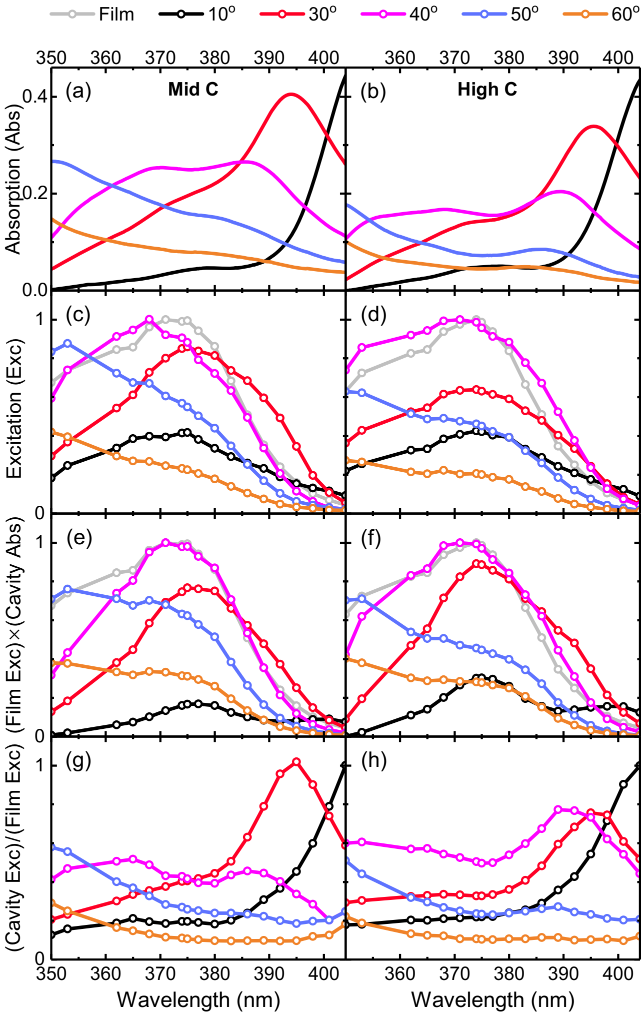

Fig. 4 | Measured and predicted excitation spectra of strongly coupled HBQ-cavities. Absorption spectra of (**a**) mid concentration (C) and (**b**) high C HBQ/PMMA cavities at various excitation angles. Excitation spectra for emission at 620 nm of (**c**) mid C and (**d**) high C HBQ/PMMA cavities as a function of excitation angle. The excitation spectrum of the films are scaled down and shown in light gray. Scaling of the film excitation spectra was done to compensate for the absence of the top mirror and to facilitate comparison. The product of the cavity absorption spectrum and film excitation spectrum for (**e**) mid C and (**f**) high C cavities. The scaling of the film excitation spectra has no effect on the shape of these product spectra. Cavity excitation spectrum divided by the film excitation spectrum for (**g**) mid C and (**h**) high C HBQ/PMMA cavities. The curves are normalized so that the highest value within a group of spectra in each panel (**c**–**h**) is scaled to one, i.e., the relative intensities of the curves are preserved to facilitate comparison. Source data are provided as a Source Data file.

Our simulations furthermore suggest that within the strong coupling regime, increasing HBQ concentration enhances the overlap at the resonance angle (Fig. 2c), and hence the efficiency of the ESIPT reaction. To verify also this finding, we measured the steady-state emission intensity at 620 nm from our HBQ cavities while exciting directly into the lower polariton at the resonance angle, i.e., the angle at which the excitation energy of bare HBQ matches the dispersion of the cavity, and the energy gap between UP and LP is minimum. These excitation wavelengths, λ_{res}, and angles, θ_{res}, are listed for each sample in Table 1. As reference, we also measured the emission from the HBQ/PMMA films with the excitation tuned to the absorption maximum ($\lambda_{ex} = 375$ nm) of the film. As in the measurements of the excitation

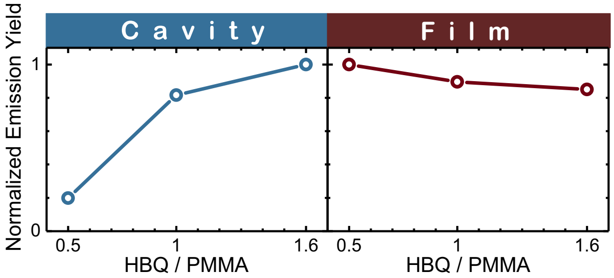

Fig. 5 | Measured emission yields as a function of coupling strength. Emission yield, η^{exp}, in HBQ-cavity systems and films as a function of HBQ/PMMA doping ratio. The emission yield is normalized to the highest value. Source data are provided as a Source Data file.

spectra, the samples were excited with ~5 ns laser pulses at a 100 Hz repetition rate. Details of these experiments are provided in the Supplementary Information (section 1.5).

We quantify the emission yield (η) in these experiments as:

$$\eta^{\text{exp}} = I(\lambda_{\text{em}})/A(\theta_{\text{res}}, \lambda_{\text{res}}) \tag{1}$$

with $I(\lambda_{\text{em}})$ the intensity at the maximum of the emission band ($\lambda_{\text{em}} = 620$ nm) and $A(\theta_{\text{res}}, \lambda_{\text{res}})$ the baseline-corrected absorption at the excitation wavelength λ_{res}, and incident angle θ_{res}. In Fig. 5, we plot the yields as a function of the HBQ/PMMA doping ratio, which is correlated with both the number of HBQ molecules within the mode volume of the cavity and the coupling strength (Table 1). The films show almost constant emission yield with only a minor decrease at higher concentrations, presumably due to quenching[47]. The absorption, $A(\theta_{\text{res}},\lambda_{\text{res}})$, was also computed with the transfer matrix method and the optical finite element method (Supplementary Information, section 1.6). While both approaches provide similar trends, the assumptions of a perfect cavity geometry is rather strong. We, therefore, only report yields, η^{exp}, that were derived from the experimental spectra. Although the relative increase of the cavity emission yield is larger than in the simulations, presumably due to the overestimation of population transfer rates in small ensembles of molecules[37], the increase is in line with our calculations. Therefore, both simulations and experiments suggest that increasing the coupling by adding more molecules, decreases the suppression by enhancing the rate at which population transfers from the lossy polariton modes into the reactive dark state manifold.

However, experiments in cavities with different Q-factors, as was done for example by Pandya et al. for investigating the effect of cavity mode lifetime on polariton-mediated exciton transport[48], would be needed to further confirm our interpretation that suppression of photo-chemistry in the strong coupling regime is due to cavity loss, rather than to a modified potential energy surface. In addition, experiments at higher HBQ concentration are needed to confirm the turn-over between the decrease and increase of losses, predicted by our simulations (Fig. 2c). However, due to the limited solubility in PMMA, either other polymer matrices or chemical modifications[49] would be required to reduce the aggregation propensity of HBQ in such experiments and reach the Rabi splittings that are necessary for observing the turn-over.

In conclusion, we have investigated how strong light-matter coupling affects an ultra-fast photo-chemical reaction that occurs on the same timescale as the cavity lifetime. While the coupling leads to the characteristic Rabi splitting in the absorption spectra, the cavity mode excitations are smeared out over so many states that their contributions are too small to significantly perturb the potential energy surface of the electronic excited state and affect the reaction dynamics. The redistribution of the cavity mode contribution is due to disorder, which suppresses the collective response, and, by localizing the excitation, reduces polaritonic effects not only on reactivity[9,39], but also on other properties, such as polariton-mediated transport[50–56]. While radiative decay from the polaritonic states in a lossy cavity can reduce the excited state population, the efficiency with which such losses suppress the reaction, depends on the competition with non-adiabatic population transfer into the molecular dark states. Since the rate of population transfer between bright and dark states is inversely proportional to the energy gap[37], this rate is determined by the overlap between the polaritonic absorption spectrum and the molecular density of states. Because this overlap depends on the number of molecules in the mode volume[18], the extent of suppression can be controlled by tuning the cavity Q-factor and the concentration. In addition, by providing additional non-reactive decay channels, cavities can also affect the excitation spectrum, and thereby selectively enhance excitation of states at the edges of the molecular excitation spectrum, where a system may be more reactive, as for example in Photoactive Yellow Protein[57]. Although we focused specifically on the effect of strong coupling on the ultra-fast ESIPT reaction in HBQ, we believe our findings, obtained by combining simulations and experiments, provide important new insights into the possibilities of altering chemistry with strong coupling in general as well as the limitations.

Methods

Experiments

Sample design and fabrication. To fabricate the samples, we first evaporated a 120 nm aluminum (Al) mirror on a glass substrate (BK7, Präzisions Glas and Optik GmbH) by e-beam evaporation. On top of this mirror, a thin molecular film with a thickness of approximately 100 nm, was deposited by spin-coating a PMMA polymer matrix doped with 10-hydroxybenzo[h]quinoline molecules (HBQ, TCI Europe N.V. Belgium, CAS# 33155-90-7). Two identical samples were always fabricated at the same time. To create an all-metal Fabry–Pérot cavity, we evaporated a 20 nm Al mirror on top of the film on one of the samples. By restricting the evaporation of the second mirror to only one of samples, the other sample remained available as a reference molecular film to compare against. Although with a 20 nm top mirror, the Q-factor of our cavities, was low ($Q \approx 17$), the asymmetric cavity geometry with a thin leaky mirror on top and a thick non-transmissive mirror at the bottom, combines sufficient light confinement for reaching the strong coupling regime, with sufficient out-coupling of the photo-product fluorescence[41].

Using transfer matrix method (TMM) and finite-difference time-domain (FDTD) modeling simulations, we further optimized the cavity geometry for the first-order cavity mode to be resonant with the first electronic absorption maximum of HBQ (375 nm) at ~40° incidence angle. An undoped reference cavity was fabricated by following the same procedure for a PMMA matrix without HBQ. Further details about the cavity design, fabrication and characterization are provided in the Supplementary Information (sections 1.1, 1.2 and 1.6).

Optical measurements. Optical measurements were carried out using a home-built goniometric setup, illustrated in Fig. S5 (Supplementary Information), that could be equipped with a wide variety of optical sources and detectors. The samples were excited with a pseudo-collimated s-polarized excitation light beam aimed at the rotation axis of the sample stage. The excitation (θ) and detection (ϕ) angles were adjusted by rotating the stage and the goniometric detection arm that was equipped with a fiber coupler (ThorLabs, F220SMA-A) connected to an optical fiber guiding the collected light into a detector.

Reflection and absorption spectra. For the reflection measurements, we excited the sample at varying incidence angles (θ) with a deuterium lamp (Cathodeon, C710) and guided the light at the reflection angle ($\phi = \theta$) via the fiber (ThorLabs, M112L02) into a spectrometer, which consisted of a monochromator (Acton, SP2150i) in combination with a CCD camera (Andor, InstaSpec IV CCD DU420-OE). The angle-resolved reflection spectra, $R(\theta, \lambda)$, were calculated as $R(\theta, \lambda) = I(\theta, \lambda)/I_0(\lambda)$, with $I(\theta, \lambda)$ being the collected signal reflected from the sample and $I_0(\lambda)$ the lamp spectrum. Without transmission through the bottom mirror (i.e., $T(\theta, \lambda) = 0$), we could compute the absorption spectrum as $A(\theta, \lambda) = 1 - R(\theta, \lambda)$. These absorption spectra were corrected for variations in the non-specular Rayleigh scattering from the top mirror surface. The details of the baseline corrections are discussed in section 1.4 of the Supplementary Information.

Fluorescence and excitation spectra. In the fluorescence measurements, the samples were excited by a fiber-coupled tunable pulsed laser (EKSPLA OPO NT230, pulse width: 3–6 ns, repetition rate: 100 Hz). The emission from the samples was coupled to a fiber optic bundle (ThorLabs, BFL200HS02) and guided into a monochromator (Acton, SP2150i) equipped with a CCD camera (Andor, IVAC CCD DR-324B-FI). A long-pass filter (Semrock, BLP01-488R-25) was placed in front of the spectrometer to avoid detecting the excitation light. The detection angle ϕ was set to 0° for all θ except for $\theta = 10°$ where ϕ was set to 30° to avoid detecting the direct reflection of the incident laser light. For the reference films, which lack dispersion, θ was set to 30° and ϕ to 0°. The collected emission intensity was normalized by the sum of the energies of all excitation pulses, which were recorded pulse by pulse with a separate sensor (Ophir PD10-C). The excitation spectra were constructed by extracting the energy-corrected emission intensities at 620 nm as a function of the excitation wavelength. Further details on these measurements and the correction of the data are provided in the Supplementary Information (Section 1.5).

Molecular dynamics simulations

Simulation model. We used the multi-scale Tavis–Cummings model, introduced by Luk et al.[33], to perform molecular dynamics (MD) simulations of 256–2048 solvated HBQ molecules strongly coupled to the confined light mode of a Fabry–Pérot cavity. In this model, we apply the Born–Oppenheimer approximation to separate the nuclear degrees of freedom, which we treat classically, from the electronic degrees of freedom and the cavity modes[58]. Within the single-excitation subspace, probed experimentally under weak driving conditions, and employing the rotating wave approximation (RWA), valid for light-matter coupling strengths below 10% of the material excitation energy[59], we model the electronic plus cavity mode degrees of freedom with the Tavis–Cummings model of quantum optics[60,61]. In the long-wavelength approximation, the interaction between the molecular excitons and the cavity modes are modeled as the inner products between the transition dipole moments and the vacuum field associated with an excitation of the Fabry–Pérot cavity mode. A concise summary of the details relevant to this work is provided in Section 2 of the Supplementary Information.

HBQ model system. The electronic ground state (S_0) of the HBQ molecules was modeled at the hybrid Quantum Mechanics/Molecular Mechanics (QM/MM) level[62,63], using density function theory with the CAM-B3LYP functional[22,23,64] in combination with a 6-31G(d) basis set[24]. The cyclohexane solvent was described with the 2016H66 parameter set of the Gromos96 force field[65]. We used time-dependent density functional theory[66] within the Tamm–Dancoff approximation (TDA)[21] in combination with the CAM-B3LYP functional and the 6-31G(d) basis set, to model the first singlet excited electronic (S_1) state of HBQ in our simulations. Further details of the HBQ simulation setup are provided in the Supplementary Information (subsection 2.3).

HBQ-cavity model. For the simulations in the cavity, 256–2048 configurations were extracted from the QM/MM ground-state trajectory and coupled to a single confined light mode with an infinite lifetime and a vacuum field strength of 0.77 MV cm^{-1} (0.00015 au). To maximize the collective coupling strength, the transition dipole moments were aligned to the cavity field. MD trajectories of 100 fs were calculated with 256, 300, 400, 512, 768, 1024, 1280 and 2048 molecules in the cavity. In these simulations, the cavity energy, $\hbar\omega_{\text{cav}}$, was tuned to be in resonance with the maximum of the HBQ absorption, which is 4.02 eV at the TDA-CAM-B3LYP/6-31G(d)//Gromos2016H66 level of QM/MM theory. In total 161 trajectories were computed, each starting in a different polaritonic eigenstate of the HBQ-cavity systems. Population transfers between states were modeled with the diabatic surface hopping method[67]. All simulations of the cavity systems were performed with Gromacs 4.5.3[68], in which the Tavis–Cummings QM/MM model was implemented[34,69], in combination with Gaussian16[70].

Data availability

All data, including raw and analyzed experimental spectra with analyzing scripts, transfer matrix and FDTD modeling data and scripts, simulations models, input files, trajectories and structures, analysis scripts and programs, including raw data, are available for download from IDA—Research Data Storage[71]. Source data are provided with this paper.

Code availability

The GROMACS-4.5.3 fork, in which the multi-scale Tavis–Cummings model used in this work, was implemented, is available for download from GitHub[72].

References

1. Hutchison, J. A., Schwartz, T., Genet, C., Devaux, E. & Ebbesen, T. W. Modifying chemical landscapes by coupling to vacuum fields. *Angew. Chem. Int. Ed.* **51**, 1592–1596 (2012).
2. Thomas, A. et al. Ground-state chemical reactivity under vibrational coupling to the vacuum electromagnetic field. *Angew. Chem. Int. Ed.* **55**, 11462–11466 (2016).
3. Thomas, A. et al. Tilting a ground-state reactivity landscape by vibrational strong coupling. *Science* **363**, 615–619 (2019).
4. Vergauwe, R. M. A. et al. Modification of enzyme activity by vibrational strong coupling of water. *Angew. Chem. Int. Ed.* **58**, 15324–15328 (2019).
5. Lather, J., Bhatt, P., Thomas, A., Ebbesen, T. W. & George, J. Cavity catalysis by cooperative vibrational strong coupling of reactant and solvent molecules. *Angew. Chem. Int. Ed.* **58**, 10635–10638 (2019).
6. Yu, Y., Mallick, S., Wang, M. & Börjesson, K. Barrier-free reverse-intersystem crossing in organic molecules by strong light-matter coupling. *Nat. Commun.* **12**, 3255 (2021).
7. Stranius, K., Herzog, M. & Börjesson, K. Selective manipulation of electronically excited states through strong light-matter interactions. *Nat. Comm.* **9**, 2273 (2018).
8. Munkhbat, B., Wersäll, M., Baranov, D. G., Antosiewicz, T. J. & Shegai, T. Suppression of photo-oxidation of organic chromophores by strong coupling to plasmonic nanoantennas. *Sci. Adv.* **4**, eaas9552 (2018).
9. Mony, J. et al. Photoisomerization efficiency of a solar thermal fuel in the strong coupling regime. *Adv. Funct. Mater.* **31**, 2010737 (2021).
10. Tropf, L. et al. Influence of optical material properties on strong coupling in organic semiconductor based microcavities. *Appl. Phys. Lett.* **110**, 153302 (2017).
11. Agranovich, V., Benisty, H. & Weisbuch, C. Organic and inorganic quantum wells in a microcavity: Frenkel-Wannier-Mott excitons hybridization and energy transformation. *Solid State Commun.* **102**, 631–636 (1997).
12. Lidzey, D. G. et al. Strong exciton-photon coupling in an organic semiconductor microcavity. *Nature* **395**, 53–55 (1998).

13. Törmä, P. & Barnes, W. L. Strong coupling between surface plasmon polaritons and emitters: a review. *Rep. Prog. Phys.* **78**, 013901 (2015).
14. Rider, M. S. & Barnes, W. L. Something from nothing: linking molecules with virtual light. *Contemp. Phys.* **62**, 217–232 (2022).
15. Galego, J., Garcia-Vidal, F. J. & Feist, J. Suppressing photochemical reactions with quantized light fields. *Nat. Comm.* **7**, 13841 (2016).
16. Garcia-Vidal, F. J., Ciuti, C. & Ebbesen, T. W. Manipulating matter by strong coupling to vacuum fields. *Science* **373**, eabd0336 (2021).
17. Agranovich, V. M., Litinskaia, M. & Lidzey, D. G. Cavity polaritons in microcavities containing disordered organic semiconductors. *Phys. Rev. B* **67**, 085311 (2003).
18. Groenhof, G., Climent, C., Feist, J., Morozov, D. & Toppari, J. J. Tracking polariton relaxation with multiscale molecular dynamics simulations. *J. Chem. Phys. Lett.* **10**, 5476–5483 (2019).
19. Kim, C. H. & Joo, T. Coherent excited state intramolecular proton transfer probed by time-resolved fluorescence. *Phys. Chem. Chem. Phys.* **11**, 10266–10269 (2009).
20. Lee, J., Kim, C. H. & Joo, T. Active role of proton in excited state intramolecular proton transfer reaction. *J. Phys. Chem. A* **117**, 1400–1405 (2013).
21. Hirata, S. & Head-Gordon, M. Time-dependent density functional theory within the Tamm-Dancoff approximation. *Chem. Phys. Lett.* **314**, 291–299 (1999).
22. Yanai, T., Tew, D. P. & Handy, N. C. A new hybrid exchange-correlation functional using the Coulomb-attenuating method (cam-b3lyp). *Chem. Phys. Lett.* **393**, 51–57 (2004).
23. Becke, A. D. A new mixing of Hartree-Fock and local density-functional theories. *J. Chem. Phys.* **98**, 1372 (1993).
24. Dunning, T. H. Basis functions for use in molecular calculations. I. Contractions of (9s5p) atomic basis sets for the first-row atoms. *J. Chem. Phys.* **53**, 2823–2833 (1970).
25. Berendsen, H., Postma, J., van Gunsteren, W., la, A. D. & Haak, J. Molecular dynamics with coupling to an external bath. *J. Chem. Phys.* **81**, 3684–3690 (1984).
26. Houdré, R., Stanley, R. P. & Ilegems, M. Vacuum-field rabi splitting in the presence of inhomogeneous broadening: resolution of a homogeneous linewidth in an inhomogeneously broadened system. *Phys. Rev. A* **53**, 2711–2715 (1996).
27. del Pino, J., Feist, J. & Garcia-Vidal, F. J. Quantum theory of collective strong coupling of molecular vibrations with a microcavity mode. *N. J. Phys.* **17**, 053040 (2015).
28. Eizner, E., Martínez-Martínez, L. A., Yuen-zhou, J. & Kéna-Cohen, S. Inverting singlet and triplet excited states using strong light-matter coupling. *Sci. Adv.* **5**, eaax4482 (2019).
29. Martínez-Martínez, L. A., Eizner, E., Kéna-Cohen, S. & Yuen-Zhou, J. Triplet harvesting in the polaritonic regime: a variational polaron approach. *J. Chem. Phys.* **151**, 054106 (2019).
30. Thomas, P. A., Tan, W. J., Kravets, V. G., Grigorenko, A. N. & Barnes, W. L. Non-polaritonic effects in cavity-modified photochemistry. *Adv. Mater.* **36**, 2309393 (2023).
31. Thomas, P. A. & Barnes, W. L. Selection bias in strong coupling experiments. *J. Phys. Chem. Lett.* **15**, 1708–1710 (2024).
32. Zeng, H. et al. Control of photoswitching kinetics with strong light-matter coupling in a cavity. *J. Am. Chem. Soc.* **145**, 19655–19661 (2023).
33. Luk, H.-L., Feist, J., Toppari, J. J. & Groenhof, G. Multiscale molecular dynamics simulations of polaritonic chemistry. *J. Chem. Theory Comput.* **13**, 4324–4335 (2017).
34. Tichauer, R. H., Feist, J. & Groenhof, G. Multiscale simulations of molecular polaritons: the effect of multiple cavity modes on polariton relaxation. *J. Chem. Phys.* **154**, 104112 (2021).
35. Vendrell, O. Collective Jahn-Teller interactions through light-matter coupling in a cavity. *Phys. Rev. Lett.* **121**, 253001 (2018).
36. Ulusoy, I. S., Gomez, J. A. & Vendrell, O. Modifying the non-radiative decay dynamics through conical intersections via collective coupling to a cavity mode. *J. Phys. Chem. A* **123**, 8832–8844 (2019).
37. Tichauer, R. H., Morozov, D., Sokolovskii, I., Toppari, J. J. & Groenhof, G. Identifying vibrations that control non-adiabatic relaxation of polaritons in strongly coupled molecule-cavity systems. *J. Phys. Chem. Lett.* **13**, 6259 (2022).
38. Flick, J., Ruggenthaler, M., Appel, H. & Rubio, A. Atoms and molecules in cavities: from weak to strong coupling in QED chemistry. *Proc. Natl Acad. Sci. USA* **114**, 3026–3034 (2017).
39. Pérez-Sánchez, J. B., Mellini, F., Giebink, N. C. & Yuen-Zhou, J. Collective polaritonic effects on chemical dynamics suppressed by disorder. *Phys. Rev. Res.* **6**, 013222 (2024).
40. Lee, I., Melton, S. R., Xu, D. & Delor, M. Controlling molecular photoisomerization in photonic cavities through polariton funneling. *J. Am. Chem. Soc.* **146**, 9544–9553 (2024).
41. Dutta, A., Tiainen, V. & Toppari, J. J. Optimizing geometry of low-Q all-metal fabry-pérot microcavity for fluorescence spectroscopy. *IOP SciNotes* **2**, 015205 (2021).
42. Purcell, E. M. Spontaneous emission probabilities at radio frequencies. *Phys. Rev.* **69**, 681 (1946).
43. Lidzey, D., Bradley, D., Armitage, A., Walker, S. & Skolnick, M. Photon-mediated hybridization of Frenkel excitons in organic semiconductor microcavities. *Science* **288**, 1620–1623 (2000).
44. Puro, R. et al. Exciton polariton-enhanced photodimerization of functionalized tetracene. *J. Phys. Chem. C.* **125**, 27072–27083 (2021).
45. Tang, Y., Stuart, A. N., van Laan, T. & Lakhwani, G. Strong light-matter coupling leads to a longer charge carrier lifetime in cavity organic solar cells. *ACS Photonics* **11**, 1627–1637 (2024).
46. George, A. et al. Controlling the manifold of polariton states through molecular disorder. *Adv. Opt. Mater.* **12**, 2302387 (2024).
47. Kwon, J. E. & Park, S. Y. Advanced organic optoelectronic materials: harnessing excited-state intramolecular proton transfer (ESIPT) process. *Adv. Mater.* **23**, 3615–3642 (2011).
48. Pandya, R. et al. Tuning the coherent propagation of organic exciton-polaritons through dark state delocalization. *Adv. Sci.* **9**, 2105569 (2022).
49. Schäfer, C., Hultmark, S., Yang, Y., Müller, C. & Börjesson, K. Room temperature dye glasses: a guideline toward the fabrication of amorphous dye films with monomeric absorption and emission. *Chem. Mater.* **34**, 9294–9302 (2022).
50. Agranovich, V. & Gartstein, Y. Nature and dynamics of low-energy exciton polaritons in semiconductor microcavities. *Phys. Rev. B* **75**, 075302 (2007).
51. Litinskaya, M. Propagation and localization of polaritons in disordered organic microcavities. *Phys. Lett. A* **372**, 3898–3903 (2008).
52. Wellnitz, D., Pupillo, G. & Schachenmayer, J. Disorder enhanced vibrational entanglement and dynamics in polaritonic chemistry. *Comm. Phys.* **5**, 120 (2022).
53. Allard, T. F. & Weick, G. Disorder-enhanced transport in a chain of lossy dipoles strongly coupled to cavity photons. *Phys. Rev. B* **106**, 245424 (2022).
54. Aroeira, G. J. R., Kairys, K. & Ribeiro, R. F. Theoretical analysis of exciton wave packet dynamics in polaritonic wires. *J. Phys. Chem. Lett.* **14**, 5681–5691 (2023).
55. Engelhardt, G. & Cao, J. Polariton localization and dispersion properties of disordered quantum emitters in multimode microcavities. *Phys. Rev. Lett.* **130**, 213602 (2023).
56. Sokolovskii, I., Tichauer, R. H., Morozov, D., Feist, J. & Groenhof, G. Multi-scale molecular dynamics simulations of enhanced energy

transfer in organic molecules under strong coupling. *Nat. Commun.* **14**, 6613 (2023).
57. Mix, L. T. et al. Excitation-wavelength-dependent photocycle initiation dynamics resolve heterogeneity in the photoactive yellow protein from halorhodospira halophila. *Biochemistry* **57**, 1733–1747 (2017).
58. Galego, J., Garcia-Vidal, F. J. & Feist, J. Cavity-induced modifications of molecular structure in the strong-coupling regime. *Phys. Rev. X* **5**, 041022 (2015).
59. Forn-Díaz, P., Lamata, L., Rico, E., Kono, J. & Solano, E. Ultrastrong coupling regimes of light-matter interaction. *Rev. Mod. Phys.* **91**, 025005 (2019).
60. Jaynes, E. T. & Cummings, F. W. Comparison of quantum and semiclassical radiation theories with to the beam maser. *Proc. IEEE* **51**, 89–109 (1963).
61. Tavis, M. & Cummings, F. W. Approximate solutions for an n-molecule radiation-field Hamiltonian. *Phys. Rev.* **188**, 692–695 (1969).
62. Warshel, A. & Levitt, M. Theoretical studies of enzymatic reactions: dielectric, electrostatic and steric stabilization of carbonium ion in the reaction of lysozyme. *J. Mol. Biol.* **103**, 227–249 (1976).
63. Groenhof, G. Introduction to qm/mm simulations. *Methods Mol. Biol.* **924**, 12489–12491 (2013).
64. Lee, C. T., Yang, W. T. & Parr, R. G. Development of the Colle-Salvetti correlation-energy formula into a functional of the electron density. *Phys. Rev. B* **37**, 785–789 (1988).
65. Horta, B. A. C. et al. A gromos-compatible force field for small organic molecules in the condensed phase: the 2016H66 parameter set. *J. Chem. Theory Comput.* **12**, 3825–3850 (2016).
66. Runge, E. & Gross, E. K. U. Density-functional theory for time-dependent systems. *Phys. Rev. Lett.* **52**, 997–1000 (1984).
67. Groenhof, G. et al. Photoactivation of the photoactive yellow protein: why photon absorption triggers a trans-to-cis isomerization of the chromophore in the protein. *J. Am. Chem. Soc.* **124**, 4228–4232 (2004).
68. Hess, B., Kutzner, C., van der Spoel, D. & Lindahl, E. Gromacs 4: algorithms for highly efficient, load-balanced, and scalable molecular simulation. *J. Chem. Theory Comput.* **4**, 435–447 (2008).
69. Sokolovskii, I. & Goenhof, G. Non-Hermitian molecular dynamics simulations of exciton-polaritons in lossy cavities. *J. Chem. Phys.* **160**, 092501 (2024).
70. Frisch, M. J. et al. *Gaussian16 Revision C.01* (Gaussian Inc., 2016).
71. Dutta, A. et al. Ultra-fast photochemistry in the strong light-matter coupling regime. IDA—Research Data Storage. https://doi.org/10.23729/11673bf8-3094-4a11-9b8c-604bef025f76 (2024).
72. Sokolovskii, I., Tichauer, R. H., Morozov, D., Feist, J. & Groenof, G. Multi-scale molecular dynamics simulations of enhanced energy transfer in organic molecules under strong coupling. *GitHub*. https://doi.org/10.5281/zenodo.8312817 (2023).

Acknowledgements

We thank Satu Mustalahti, Ossi Hakamaa, Mikael Kautto, Oskar Celik, Ruth H. Tichauer, Pasi Myllyperkiö, Tatu Kumpulainen, Thomas Fuhrmann-Lieker, and Thomas Kusserow for their assistance at various stages of the project. This work was supported by the Academy of Finland via Research projects (Grants Nos. 323996 and 332743 to G.G., Nos. 323995, 289947 and 350797 to J.J.T.) and University profiling funding (Profi4 to University of Jyväskylä), with contributions from the Finnish Cultural Foundation (Grant No. 00231164 to J.J.T. and G.G.) and the Estonian Research Council (Grant No. PSG406 to S.P.). We also thank the Center for Scientific Computing (CSC-IT Center for Science) for generous computational resources for G.G.

Author contributions

G.G. and J.J.T. conceptualized the project and acquired funding. L.D. and V.T. developed the optical measurement setup. A.D., V.T., L.D., N.M. and H.A.Q. carried out the measurements. A.D., V.T. and H.A.Q. fabricated the samples. I.S. and G.G. performed the molecular dynamics simulations. D.M. performed quantum chemistry calculations. V.T. and A.D. performed TMM and FDTD computations. S.P. performed optical finite element modeling. All authors contributed to the interpretation of the data. The manuscript was written by G.G., J.J.T. and A.D. with input from all authors. All authors reviewed, commented on the manuscript and approved the final version.

Competing interests

The authors declare no competing interests.

Additional information

Supplementary information The online version contains supplementary material available at https://doi.org/10.1038/s41467-024-50532-5.

Correspondence and requests for materials should be addressed to Gerrit Groenhof or J. Jussi Toppari.

Peer review information *Nature Communications* thanks Hsing-Ta Chen, Joel Yuen-Zhou, and the other, anonymous, reviewers for their contribution to the peer review of this work. A peer review file is available.

Reprints and permissions information is available at http://www.nature.com/reprints